WOOD RESEARCH **doi.org/10.37763/wr.1336-4561/71.4.568583**
e-ISSN 2729-8906
71(4): 2026 568-583 pp.

ANALYSIS OF STRUCTURAL CHARACTERISTICS OF BACTERIAL NANOCELLULOSE SYNTHESIZED USING BEECHWOOD HYDROLYSATE

EDUARD HORBAN[1], PETRA OLEJNÍKOVÁ[2], ALBERT RUSS[1], MICHAL ŽITŇAN[3], ŠTEFAN BOHÁČEK[1], VLADIMÍR IHNÁT[1], ANDREJ PAŽITNÝ[1], MONIKA STANKOVSKÁ[1], JÁN TALÁBA[1]
[1]PULP AND PAPER RESEARCH INSTITUTE, SLOVAKIA
[2]SLOVAK UNIVERSITY OF TECHNOLOGY IN BRATISLAVA, SLOVAKIA
[3]ALEXANDER DUBČEK UNIVERSITY OF TRENČÍN, SLOVAKIA

(RECEIVED JUNE 2026)

ABSTRACT

In this study, a comprehensive structural analysis to increase yield, optimize cultivation parameters, and evaluate bacterial nanocellulose (BNC) organization using two types of media was conducted. Cultivation of *Komagataeibacter xylinus* (*K. xylinus*) DSM 46591 was performed in an alternative beechwood hydrolysate medium (BH) and the standard Hestrin–Schramm medium (HS) over a period of 72–432 h. High–performance liquid chromatography (HPLC) confirmed the successful extraction of glucose, xylose, and associated compounds from the wood. Fourier–transform infrared spectroscopy (FTIR) revealed visible changes in supramolecular structure in BH, resulting in a 12.8% decrease in the lateral order index (LOI: 0.748 → 0.652) and a simultaneous increase in the hydrogen bond index (HBI: 0.997 → 1.111) in comparison with HS. X–ray diffraction (XRD) showed that BH promotes the synthesis of a combination of cellulose triclinic (Iα) and monoclinic (Iβ) with a high crystallinity index (CI = 86%), while sterically limiting lateral crystallite growth (the crystallite sizes (CS) of the (002) crystallographic plane were 6.1–6.5 nm for BH vs. 6.7 nm for HS). Scanning electron microscopy (SEM) confirmed that, in BH, this resulted in a reticulated, interconnected three–dimensional nanofibrillar matrix with preserved capillary porosity. In contrast, the HS samples showed pore clogging, denser fibre packing, and layer stacking.

KEYWORDS: Bacterial nanocellulose (BNC), beechwood hydrolysate (BH), enzymatic hydrolysis (EH), Hestrin–Schramm medium (HS), *Komagataeibacter xylinus (K. xylinus)* DSM 46591.

INTRODUCTION

The genus of cellulose–producing bacteria *Komagataeibacter (Acetobacter)* is capable of synthesizing BNC, a high–purity, nanostructured biopolymer characterized by an interconnected three–dimensional fibrillar network, superior water–holding capacity, and

exceptional mechanical strength (Ross et al. 1991). Unlike plant–derived cellulose, BNC is synthesized without lignocellulosic impurities (de Amorim et al. 2020). Biosynthesis occurs as the membrane–embedded cellulose synthase complex (Bcs) polymerizes UDP–glucose into β–D–1,4–glucan chains for extracellular extrusion (Gorgieva & Trček 2019; Ross et al. 1991).

However, large–scale commercial adoption remains constrained by the high cost of HS (Tsouko et al. 2015). Consequently, utilizing low–cost agricultural and industrial waste streams – specifically, BH, rich in glucose, xylose, and soluble lignocellulosic fractions – offers a sustainable route to reduce production costs while actively altering the physicochemical properties of the polymer (Chorozian et al. 2026; Mohammadkazemi et al. 2015; Nitzsche et al. 2020).

Qualitative and quantitative HPLC monitoring of BH obtained after enzymatic hydrolysis (EH) is essential for characterizing the potential culture medium. The subsequent synthesis process of BNC spontaneously leads to crystallization, resulting in a mixture of the allomorphic forms of native cellulose I – Iα and Iβ (Atalla 1984; Sugiyama et al. 1991). The XRD confirms phase purity and detects potential allomorphic transitions. The CS along the (002) crystallographic plane, calculated using the Scherrer equation, directly reflects the initial width of the individual nanofibrils during the early stages of biosynthesis (French 2014; Segal et al. 1952). Concurrently, structural order at the molecular level can be quantified via FTIR using the LOI (A_{1427}/A_{898}) and the HBI (A_{3335}/A_{1337}), which serve as direct indicators of packing regularity and interchain hydrogen bonding strength (Morales et al. 2025; Nelson 1964; Popescu et al. 2007). From a morphological perspective, the use of SEM data enabled a comparison of the formation patterns of the three–dimensional nanofibrillar network.

The primary objective of the study was to demonstrate the functionality of the developed method for producing BH and synthesizing BNC of better quality – in terms of physicochemical parameters – compared to HS, as well as to stabilize cultivation conditions.

MATERIAL AND METHODS

Reagents

Culture media: bacteriological agar (Th. Geyer GmbH & Co. KG, Renningen, DE), D–glucose anhydrous (Centralchem, s.r.o., Bratislava, SK), yeast extract (Carl Roth GmbH, Karlsruhe, DE), peptone GMO–free (Mushroom Research Center GmbH, Innsbruck, AUT), disodium phosphate dodecahydrate (Lachema, s.r.o., Brno, CZ), citric acid monohydrate anhydrous (Centralchem, s.r.o., Bratislava, SK). Water was distilled and deionized using a DI–PAK® Purification Pack cartridge with a Milli–DI® system (Merck KGaA, Darmstadt, DE). Sulfuric acid, glucose, xylose, arabinose, formic acid, acetic acid, levulinic acid, hydroxymethylfurfural, furfural, and ethanol (Centralchem, s.r.o., Bratislava, SK) were used for HPLC analyses. Cellic® CTec3 (Novozymes A/S, Lyngby, DE) was used for EH.

Bacterial strain, media, and cultivation conditions

The microorganism used in this study was *K. xylinus* DSM 46591. It was purchased from the Leibniz Institute (DSMZ GmbH, Braunschweig, DE). A lyophilized culture of *K. xylinus* DSM 46591 was reconstituted and activated according to the supplier's instructions. Primary activation was performed on agar plates in DSMZ medium #105 at 28.5°C, pH 7.0, for 7 days

under static aerobic conditions (DSMZ GmbH, 2007).

As a standard, HS (glucose: 20 g/L, peptone: 5 g/L, yeast extract: 5 g/L, disodium phosphate: 2.7 g/L, and citric acid: 1.15 g/L), pH 6.0, was prepared (Akintunde et al. 2022; Hestrin 1954). The culture medium was sterilized at 121°C and 120–125 kPa for 20 min. Sterile 250–mL Fisher Brand flasks were filled with 90 mL of cooled, fresh HS. Direct inoculation of growing pure bacterial cultures from DSMZ #105 agar nutrient medium was performed using a standard 1.5 mm inoculation loop. Five calibrated loops of biomass were aseptically transferred from dense 6–day–old colonies (144 h) into Fisher Brand flasks containing 90 mL of HS and stirred. Cultivation was carried out at 28.5°C, pH 6.0, under static aerobic conditions using 18 independent culture flasks for each medium type to establish a chronological profile of BNC generation. The experimental matrix included six process durations (3, 6, 9, 12, 15, and 18 days), evaluated in triplicate. At each sampling threshold, three vessels were used to isolate BNC hydrogels.

An alternative growth medium was prepared using the hydrolysate of beech sawdust (*Fagus sylvatica*) with 12% moisture content, originating in northern Slovakia, as the main carbon source. Sawdust preliminary processing was carried out by mechanical dry grinding to a fraction of 0.7 mm in a Brabender mill (Brabender®, GmbH& Co. KG, DE). Beech sawdust was impregnated with water so that the final relative humidity of the samples during the steam explosion was 85% by weight. The samples of mass 100 g a.s. were finally pretreated in a 2 L stainless steel batch reactor for steam explosion (STEX) pretreatment (Amar Equipments Pvt. Ltd., IN). The reactor was set to a temperature of 220°C. At the same time, an additional pressure of 10 bar was added to increase the effect of the blast. The retention time for each thermo–hydro–mechanical experiment was 10 min. A total of 5 shots were performed, with an average temperature of 222.4°C (S_{dev} = 4.72°C) and an average pressure of 35.14 bar (S_{dev} = 2.5 bar). After the steam explosion, the samples were refrigerated before further use. Each sample was then leached in 2 L of hot water to release extractable substances. After 2 h of leaching, the sample was rinsed 5 times with clean water. The rinsed fibres were centrifuged at 4.110 rpm for 17 min and decanted. A total of 850 g of sample with a dry matter content of approximately 30% was obtained.

After STEX pretreatment, the samples were subjected to EH. The EH was carried out using the cellulase complex Cellic® CTec3 (Novozymes A/S, Lyngby, DE) with a recommended dosage of 15% by weight of enzyme suspension (15 g Cellic® CTec3/100 g suspension). The pH was adjusted with NaOH solution (10% wt.) to pH = 5.0 at 50°C. After 72 h, the 8 Fisher Brand flasks (500 mL) with the suspension were removed from the incubator. Samples were boiled for 10 min in a water bath to deactivate the enzyme. The obtained BH in liquid form was centrifuged at 12000 rpm for 30 min. The clear supernatant was analysed by HPLC, and it was subsequently diluted with distilled water to the final concentration of fermentable sugars at 20.0 g/L, which was consistent with the carbon source concentration in HS. The BH was supplemented with standard HS nutrients to standardize the cultivation parameters and isolate the carbon sources as the main experimental variable (peptone: 5 g/L, yeast extract: 5 g/L, disodium phosphate: 2.7 g/L, and citric acid: 1.15 g/L), pH 6.0. The medium was autoclaved at 121°C and 120–125 kPa for 20 min.

Collection, purification, and preparation of BNC

The resulting BNC hydrogel membranes were aseptically removed from the culture media. The pH of the culture media was measured after cultivation. The membranes were placed in glassware and cleaned with a 0.1 M NaOH solution at 80°C for 2 h. After 2 h (in case of thicker membranes, after 3 h), the membranes were rinsed with distilled water for 10 min and then cleaned again with a fresh 0.1 M NaOH solution for 1 h. The membranes were then placed in Petri dishes with distilled water and rinsed 5–6 times with distilled water (10 min/cycle) or until a neutral pH was achieved. Their pH was measured and fixed at 6.0–7.0. The prepared membranes were placed in distilled water and stored in a refrigerator at 4°C.

The resulting membrane triplicates were air–dried in air with tweezers for 1 min to remove excess surface water. Residual moisture was removed using Filter 389 high–quality filter paper circles (Ahlstrom Oyj, Espoo, FI). The membrane was placed between two filter paper circles and then pressed together using wooden blanks. This process was repeated until the filter paper circles remained dry. The BNC membranes were placed in a Venticell 22 forced–air drying oven (MMM Medcenter Einrichtungen GmbH, Planegg, DE) and dried at 30 °C until constant weight was achieved. The dried BNC membrane films were weighed and used for further analytical methods.

Determination of yield

Quantitative bioprocess parameters were determined in triplicate (three independent biological replicates for each cultivation time interval). BNC yield (g/L), the main kinetic parameter, reflecting the mass of the target product per unit volume of medium, was calculated according to Eq. 1. Volumetric productivity (g/L*day) represents the average rate of polymer accumulation over the entire fermentation period (Eq. 2):

$$p = \frac{W_{dry}}{V} \quad (1)$$

$$Q_p = \frac{P}{t} = \frac{W_{dry}}{V \times t} \quad (2)$$

where: W_{dry} – dry mass of the membrane dried to constant weight; V – volume of liquid medium in one vessel; t – total duration of cultivation.

Hydrophilic properties

To determine the moisture content (MC) and water–holding capacity (WHC), never–dried BNC membrane samples, removed from distilled water, were held in air with tweezers for 1 min to remove excess surface water (BNC wet). Then the samples were dried until completely free of water and weighed again (BNC dry). The MC, which reflects the mass fraction of water (free and bound) in the never–dried BNC hydrogel, was calculated using Eq. 3 (Chandrasekaran et al. 2017). The WHC, which corresponds to the retention of the liquid phase by one gram of dry polymer matrix, was calculated using Eq. 4 (Feng et al. 2015):

$$MC = \frac{BNC_{wet} - BNC_{dry}}{BNC_{wet}} \times 100\% \quad (3)$$

$$WHC = \frac{BNC_{wet} - BNC_{dry}}{BNC_{dry}} \quad (4)$$

Physiological properties

The pH of the medium (*ΔpH*) was measured using a Radelkis OP–211/1 digital pH meter (Radelkis, Budapest, HU) to assess the intensity of carbohydrate by–product oxidative metabolism and was calculated using Eq. 5:

$$\Delta pH = pH_{initial} - pH_{final} \quad (5)$$

Analytical methods

The concentration of monosaccharides (glucose, xylose), organic acids (acetic acid, gluconic acid), and inhibitors (5–hydroxymethylfurfural, furfural) in BH was determined by HPLC with a Rezex ROA H+ column (Sluiter et al. 2008) during and after the process of EH. The mobile phase consisted of 0.005 M sulfuric acid in deionized water. Analyses were performed at 30°C with the mobile phase flow rate set at 0.5 mL/min. Shodex RI–101 refractometric detector was used to detect analytes, and the Clarity program from Data Apex was used to collect and evaluate chromatograms of samples.

The FTIR was used to characterize the chemical structure and functional groups of dried BNC samples using a Nicolet iS10 FTIR spectrometer (Thermo Fisher Scientific, USA) equipped with a diamond crystal. Spectra were recorded over a wavenumber range of 4000 to 500 cm^{-1} with a resolution of 4 cm^{-1} and 64 scans per sample. Baseline correction of the obtained spectra was performed using OMNIC v. 8.0.

Crystalline phases and crystallite size were analysed using XRD on a PANalytical Empyrean diffractometer (Empyrean, Almelo, NL) with Cu Kα radiation (λ = 1.5405 A, 45 kV, 40 mA) and a PIXcel 3D detector. Diffraction patterns were collected at a scan rate of 1.3 ◦/min and analysed using HighScore Plus software (v.5.1.0, PANalytical) with the PDF–2 database (Release 2022). To evaluate CI, the peak height method was used (Park et al. 2010) (Fig. 5b). The CS was calculated using the Scherrer method (Scherrer 1918).

The micromorphology of BNC films was assessed using a Thermo Scientific™ Prisma™ E SEM (Thermo Fisher Scientific, Waltham, MA, USA) operating at an accelerating voltage of 2–5 kV. Dried membrane sections from the centre and periphery were mounted on aluminium holders using double–sided conductive carbon tape and then examined microscopically without additional surface treatment.

Statistical analysis

To mathematically describe the kinetics of BNC accumulation and estimate the parameters of the cultivation process in HS and BH, a reduced two–parameter version of the modified Gompertz model in the Zwietering formulation was employed (Eq. 6) (Amru et al. 2018; Nugroho et al. 2022; Zwietering et al. 1990). The lag phase parameter (λ) was fixed to zero. The experimental data points obtained from Day 0 to Day 15 were fitted via non–linear regression analysis. The data collected on Day 18 were explicitly excluded from the regression fitting due to post–peak non–monotonic polymer degradation and culture lysis, which fall outside the sigmoidal growth boundaries of the Gompertz equation:

$$y = A \times \exp\left\{-exp\left[1 - \frac{\mu_m \times e \times t}{A}\right]\right\} \quad (6)$$

where: y – the current cumulative yield of BNC at time t; A (g/L) — the maximum asymptotic potential of BNC biosynthesis; μ_m (g/L × day) – the maximum production rate of BNC; e – Euler's mathematical constant ≈ 2.7183; t – independent variable of cultivation time.

The mathematical reliability of the model was quantitatively evaluated using the linear coefficient of determination (R^2), the adjusted coefficient of determination ($Adj.\ R^2$), and the root mean square error ($RMSE$), expressed as the standard deviation of the residuals (Motulsky & Christopoulos 2004; Motulsky & Ransnas 1987). The calculated kinetic parameters – A and μ_m – are presented alongside their corresponding 95% confidence intervals (95% CI), strictly computed using the asymmetrical profile likelihood method to account for non–linear parameter constraints ($A \geq 0; \mu_m \geq 0; \lambda = 0$) (Meeker 1998). The structural adequacy and homoscedasticity of the nonlinear regression were verified by analysing the distribution of the regression errors (residuals). The normal distribution of the residuals was rigorously assessed using the Shapiro–Wilk normality test, with the statistical significance threshold set at $\alpha = 0.05$ (Shapiro & Wilk 1965; Wayne 2013). All operations were performed using GraphPad Prism version 11.0.2 (100).

RESULTS AND DISCUSSION

Chemical composition of BH

The chemical composition of BH at different stages of processing, including alkaline leaching, washing, and subsequent hydrolysis (at 43 and 70 h), was quantitatively profiled using HPLC. The dynamic changes in the concentrations of fermentable monosaccharides and other byproducts are summarized in Tab. 1.

Tab. 1: Dynamic profiling of carbohydrates and degradation byproducts during stages of BH preparation.

Processing stage	Carbon sources (g/L)		Organic acids & inhibitors (g/L)				
	Glucose	Xylose	Arabinose	Formic acid	Acetic acid	Levulinic acid	Ethanol
After leaching	0.56	1.87	0.65	1.28	2.34	0.24	3.57
After washing	ND	0.09	0.09	0.03	0.11	0.01	0.09
EH (43 h)	57.50	21.10	ND	0.09	2.44	ND	ND
EH (70 h)	68.10	22.50	ND	0.18	2.65	ND	ND

**ND: Not detected (below the limit of analytical detection).*

The leaching stage enabled the dissolution and removal of readily soluble components (sugars, organic acids, and ethanol). The subsequent washing stage demonstrated high purification efficiency: the acetic acid concentration decreased by 95.3% (from 2.34 to 0.11 g/L), and formic acid by 97.7% (from 1.28 to 0.03 g/L), which prevented the initial decomposition products from entering the main EH phase. As a result of EH, after 70 h, 370 mL of concentrated sugar syrup was obtained with a glucose content of 68.10 g/L and xylose of 22.50 g/L (total sugar concentration of 90.60 g/L; ratio 3:1). The absence of levulinic acid and ethanol, combined with an insignificant content of formic acid (0.18 g/L), confirms high selectivity of EH. Progressive deacetylation of beechwood glucuronoxylan during EH resulted in an acetic acid accumulation of 2.65 g/L at 70 h. Because raw BH had a high sugar density (90.60 g/L), the substrate was standardized to a target total carbohydrate concentration of 20 g/L

before inoculation. This 4.53–fold dilution proportionally reduced the final acetic acid content to approximately 0.58 g/L.

Dynamics of BNC production

In the comparison of the physiological response of *K. xylinus* DSM 46591 to BH and HS over an 18–day cultivation period, the major macroparameters of BNC accumulation and pH dynamics are listed in Tab. 2. The initial cultivation phase (3 days) was characterized by a significant increase in BNC yield in BH to 0.441 ± 0.033 g/L, more than twice the yield observed in HS during the same period (0.214 ± 0.019 g/L). This trend in polymer accumulation persisted throughout the 15th day of fermentation. The maximum BNC concentration in BH was recorded on the 15th day (1.411 ± 0.178 g/L), whereas in HS it was 0.813 ± 0.060 g/L.

Tab. 2: The BNC yield, pH of media, volumetric productivity, MC, and WHC for each of the 6–time intervals (mean ± standard error, n = 3).

Medium	Time	Yield (g/L)	Q_p (g/L*day)	MC (%)	WHC (g/g)	pH
HS	0 days	–	–	–	–	6.00 ± 0.00
BH		–	–	–	–	6.00 ± 0.00
HS	3 days (72h)	0.214 ± 0.019	0.071 ± 0.006	99.363 ± 0.012	155.93 ± 2.87	4.91 ± 0.28
BH		0.441 ± 0.033	0.147 ± 0.011	99.118 ± 0.033	112.51 ± 4.18	5.37 ± 0.06
HS	6 days (144h)	0.415 ± 0.074	0.069 ± 0.012	98.812 ± 0.126	83.85 ± 9.14	4.44 ± 0.02
BH		0.579 ± 0.015	0.096 ± 0.003	99.192 ± 0.043	123.07 ± 6.72	5.56 ± 0.05
HS	9 days (216h)	0.606 ± 0.171	0.067 ± 0.019	98.365 ± 0.124	60.38 ± 4.59	4.37 ± 0.08
BH		0.874 ± 0.077	0.097 ± 0.009	98.934 ± 0.035	92.90 ± 3.01	5.70 ± 0.07
HS	12 days (288h)	0.613 ± 0.044	0.051 ± 0.004	98.601 ± 0.099	70.68 ± 4.90	4.40 ± 0.04
BH		1.364 ± 0.149	0.114 ± 0.012	98.766 ± 0.046	80.09 ± 2.95	5.54 ± 0.05
HS	15 days (360h)	0.813 ± 0.060	0.054 ± 0.004	98.221 ± 0.098	55.34 ± 3.03	4.89 ± 0.03
BH		1.411 ± 0.178	0.094 ± 0.012	98.782 ± 0.030	81.15 ± 1.99	5.70 ± 0.28
HS	18 days (432h)	0.510 ± 0.043	0.028 ± 0.002	99.054 ± 0.097	105.39 ± 10.51	5.04 ± 0.22
BH		0.841 ± 0.105	0.047 ± 0.006	98.381 ± 0.230	61.54 ± 8.27	6.30 ± 0.22

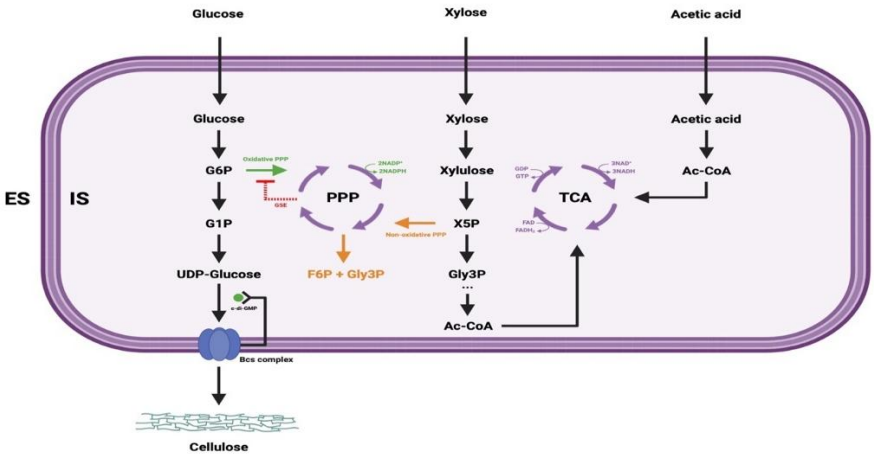
The dynamics of Q_p clearly demonstrate the BH's efficiency. Peak productivity values for BH are observed on the 3rd day (0.147 ± 0.011 g/L*day) and on the 12th day (0.114 ± 0.012 g/L*day). From a biochemical point of view, such a high rate of glucan chain polymerization in BH can be explained by the effect of glucose utilization mainly in the anabolic cascade or a glucose–sparing effect. The presence of xylose in BH at a 1:3 ratio, as well as a moderate concentration of acetate, allows the strain to utilize these substances to generate energy. Considering that xylose is not utilized in its pure form as a precursor for the synthesis of BNC glucan chains, it is used as an energy regulator within the nonoxidative branch of the pentose phosphate pathway (PPP). This flow feeds downstream glycolysis and the citric acid cycle (TCA) to produce adenosine triphosphate (ATP) and nicotinamide adenine dinucleotide (NADH), preserving glucose primarily for BNC biosynthesis. Furthermore, gluconeogenic recycling of fructose–6–phosphate derived from xylose back to glucose–6–phosphate (G6P) indirectly promotes the regeneration of cellular nicotinamide adenine dinucleotide phosphate (NADPH) via oxidative PPP (Domingues et al. 2021; Xu et al. 2019).

Another energetic parameter that could determine the kinetic advantage of BH over HS is

the presence of acetic acid at non–inhibitory concentrations. Acetate penetrates the cytoplasmic membrane of bacterial cells, is converted to acetyl–CoA, and enters the TCA cycle. This leads to the production of NADH, flavin adenine dinucleotide, and guanosine triphosphate or ATP (Fei et al. 2023; Montenegro–Silva et al. 2024).

The third factor (Fig.1) enables the distribution of metabolic fluxes. In HS, the presence of glucose alone or in excess leads to the overproduction of gluconic acid via the glucose dehydrogenase complex (GDH), which accelerates the decrease in pH to values critical for the function of the Bcs. In BH, organic acids and xylose are present. First, the catabolism of organic acid salts consumes intracellular protons, thereby compensating for external acidification of the medium and shifting the pH to the range of 5.3–5.7. Second, the balanced 3:1 monosaccharide ratio offsets the kinetic need to discharge excess reducing equivalents through the GDH shunt. This prevents the loss of the glucose portion of the substrate and ensures consistently high polymer synthesis throughout the exponential growth period (Kuo et al. 2016; Montenegro–Silva et al. 2024). On the other hand, xylose can also be converted via the GDH complex to xylonate, which can also acidify the medium. However, a xylose ratio of 1:3 simply prevents this effect from manifesting as a macroparameter.

Fig. 1: Proposed scheme of the main metabolic steps of distribution of carbon flows and acetic acid during BNC biosynthesis by K. xylinus DSM 46591 in BH. The green arrow shows the normal G6P pathway through the oxidative branch of PPP, followed by the generation of 2NADPH. The orange arrows show the pathways for X5P entry into the nonoxidative branch of PPP, followed by the formation of F6P and Gly3P. The red dotted arrow shows feedback inhibition via GSE, driven by the high reducing potential generated by xylose and acetate catabolism.



Abbreviations: ES – extracellular space; IS – intracellular space; G6P – glucose–6–phosphate; G1P – glucose–1–phosphate; UDP–Glucose – uridine diphosphate glucose; F6P – fructose 6–phosphate; c–di–GMP – cyclicdiguanylate; Bcs complex – bacterial cellulose synthase complex; X5P – xylose–5–phosphate; Gly3P – glyceraldehyde–3–phosphate; Ac–CoA – acetyl–CoA; GSE – glucose–sparing effect. Created with BioRender.

Kinetics of BNC production

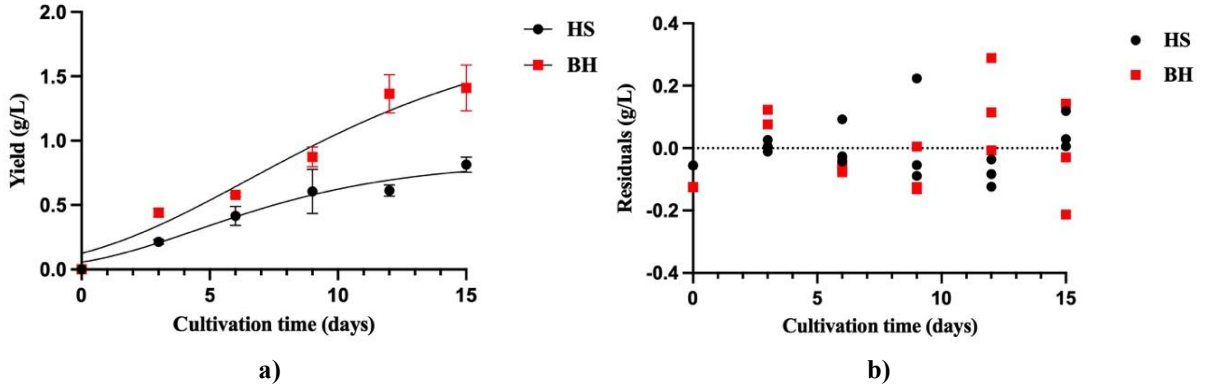
The initial test of the three parameters without restrictions on λ demonstrated that the 95% CI spans negative values (from −1.810 to 2.044 days for HS and from −1.051 to 2.433 days for BH). Mathematically, this indicates that the parameter λ is statistically indistinguishable from zero ($p > 0.05$). The introduced constraint $\lambda = 0$ eliminated overparameterization of the model,

which was confirmed by an increase in *Adj.* R^2 (it increased from 0.904 to 0.909 for HS and from 0.935 to 0.935 for BH). This adjustment significantly improved the precision of the remaining parameters, narrowing, for example, the width of the 95% CI for μ_m by more than two-fold.

From a physiological perspective, the lack of a mathematically determinable λ can be explained by two main factors. The first is based on the metabolic activity of the 6–day *K. xylinus* DSM 46591 culture, which does not require lengthy enzymatic adaptation. The second is explained by the specific 3–day sampling interval, which could have masked any shorter–timescale lag phase. The sampling specificity was based on the minimum time required for the formation of a physically quantifiable BNC hydrogel on the medium surface. In this case, increasing the sampling frequency would have been impossible because the hydrogel remained immature for up to 3 days.

Overall, the two–parameter Gompertz model (Fig. 2) demonstrated a high fit in both media, yielding high R^2 values (≥ 0.909). Model accuracy was further supported by low $RMSE$ values (0.084 g/L for HS and 0.127 g/L for BH). Considering the maximum accumulation yield, the $RMSE$ was only 10.0% (HS) and 6.7% (BH) of A, demonstrating low random error and high predictive performance. The slightly higher absolute $RMSE$ value in BH (0.127 vs. 0.084 g/L) corresponds to a higher overall BNC synthesis.

Fig. 2: Kinetic analysis of BNC accumulation by K. xylinus DSM 46591 in HS and BH during 15 days of static cultivation: a) BNC accumulation kinetics approximated by a reduced two–parameter version of the modified Gompertz model in the Zwietering formulation (λ = 0). Dots represent mean values ± standard deviation (n = 3); solid lines are nonlinear regression curves; b) Residual plot illustrating the distribution of experimental data deviations relative to the zero line (dashed line, Y = 0).



Abbreviations: HS – Hestrin–Schramm medium; BH – beechwood hydrolysate.

A progressive monotonic increase in BNC yield up to day 15 is also observed in Fig. 2a, which directly correlates with the Gompertz model. To confirm the statistical adequacy, a residual analysis was performed (Fig. 2b). The residual values for both media were uniformly and randomly dispersed around the horizontal zero line ($Y = 0$) over the entire 15–day interval. The residuals for HS were within a narrow range from −0.12 to +0.22 g/L, while for BH a proportionally wider spread was observed from −0.21 to +0.29 g/L, which corresponds to a higher absolute mass of biosynthesis. The absence of U–shaped or other systematic trends

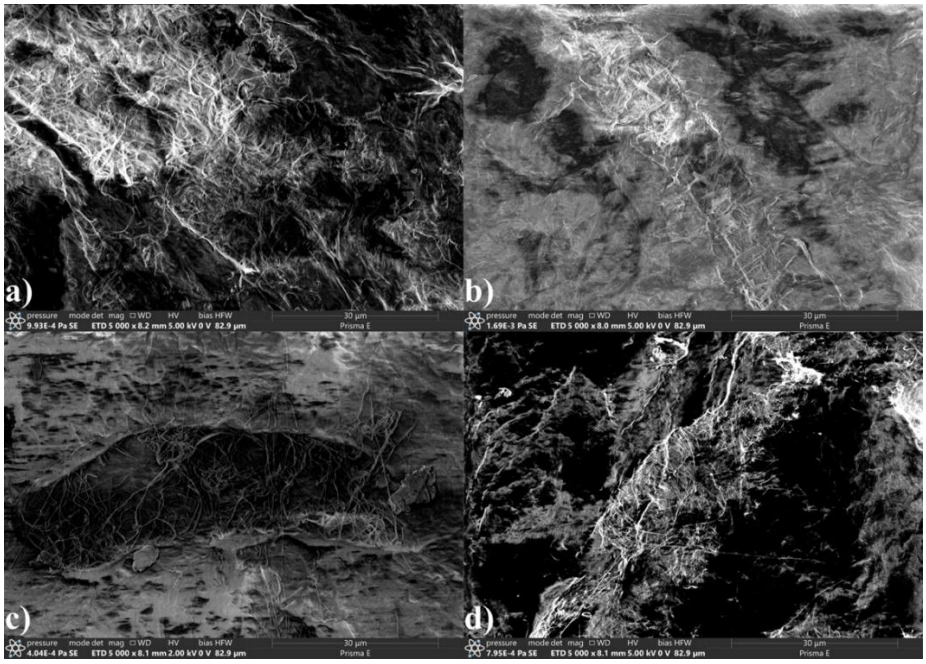
confirms homoscedasticity and proves that the selected method does not introduce a systematic error in the parameter calculations.

Comparative analysis of kinetic parameters revealed significant metabolic benefits of using BH. The μ_m for BNC production in BH reached 0.107 g/L*day (95% CI: 0.096–0.120), representing an increase of 57.4% compared to HS of 0.068 g/L*day (95% CI: 0.057–0.084). The A parameter reached 1.893 g/L (95% CI: 1.464–3.081) in BH, exceeding HS (0.842 g/L) by 2.25 times. It is important to note that this is the theoretical maximum biosynthetic potential of the culture in its productive phase before the onset of degradation processes (up to day 18).

SEM

The SEM micrographs (Fig. 3) revealed differences in the spatial architecture between BNC synthesized in HS (Figs. 3a,b) and BH (Figs. 3c,d). At 72 h, HS generated a compact, densely entangled three–dimensional network characterized by extensive lateral aggregation of elementary microfibrils into thick ribbons. In contrast, BNC formed in BH presented a highly porous, open–mesh architecture composed of finer, non–aggregated individual nanofibrils. This morphological divergence persisted through the active growth phase at 216 h. While the HS matrix consolidated into a continuous, low–porosity fibrillar mat due to uninterrupted ribbon deposition, the BH matrix maintained an interconnected, highly capillary–porous framework surrounded by an ultra–fine secondary microfibrillar web.

Fig. 3: Surface SEM micrographs illustrating the spatial network architecture of BNC dried membranes harvested during the stage of active biosynthesis in HS 72 h (a), 216 h (b), and BH 72 h (c), 216 h (d).

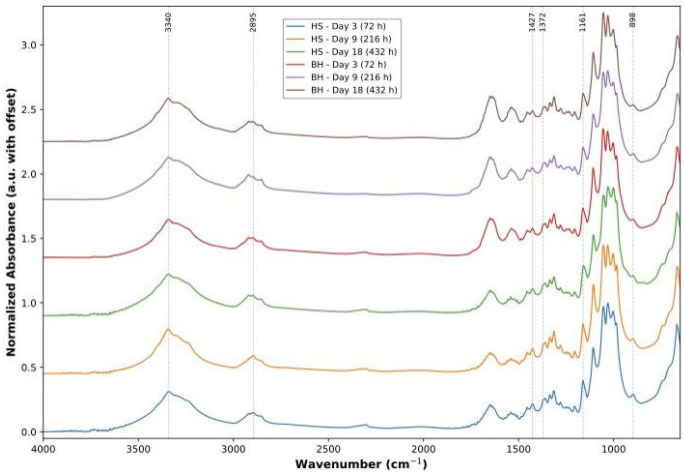


FTIR

The quantitative analysis of FTIR spectra (Fig. 4) independently validated the crystallographic alterations identified by XRD. During the active biosynthesis phase (72–216 h), LOI of BNC synthesized in BH exhibited a reduction from 0.75 to 0.65 (a 12.8%

decrease). In contrast, HS maintained relative structural stability, with its LOI dropping by merely 2.6% (from 0.72 to 0.70). This pronounced reduction in BH's LOI corroborates the Scherrer analysis in the XRD section, confirming that high production rates $\mu_{max} = 0.107\ day^{-1}$ coupled with steric hindrance from hydrolysate co–substituents yield a less laterally ordered, finer crystalline assembly.

Fig. 4: Comparative FTIR spectra of BNC synthesized in HS and BH on days 3, 9, and 18 (72, 216, 432 h). Dashed lines highlight characteristic functional bands of native cellulose I: –OH stretching (3340 cm^{-1}), –CH stretching (2895 cm^{-1}), crystalline –CH$_2$ bending (1427 cm^{-1}), –CH bending (1372 cm^{-1}), asymmetric C–O–C bridge stretching (1161 cm^{-1}), and β–1,4–glycosidic linkage deformation (898 cm^{-1}).



Abbreviations: HS – Hestrin–Schramm medium; BH – beechwood hydrolysate.

Intriguingly, at prolonged incubation (432 h), BNC from BH exhibited a sharp rebound in both LOI (0.81) and total crystallinity index (TCI = 1.88) (Tab. 3). This structural phenomenon is attributed to the death phase of *K. xylinus* DSM 46591, in which enzymatic or hydrolytic degradation occurs. The enzymatic process can be attributed to the action of enzymes from the glycoside hydrolase family – namely, endo–β–1,4–glucanases (such as BcsZ) encoded by the *bcs* operon. Hydrolytic degradation, specifically non–enzymatic acid hydrolysis, is driven by the accumulation of organic acid byproducts, the protons of which can selectively cleave amorphous domains. These, in turn, lead to a pellicle compaction of the film, artificially elevating the crystalline–to–amorphous absorbance ratio. Furthermore, HBI in BH increased from 1.00 at 72 h to 1.11 at 432 h, indicating increased intermolecular hydrogen–bonding density as the BNC matrix densifies during extended cultivation.

Tab. 3: The FTIR absorption optical density values (A_{1427}, A_{898}) and calculated supramolecular indices (LOI, TCI, HBI) of BNC synthesized in HS and BH on days 3, 9, and 18 (72, 216, 432 h).

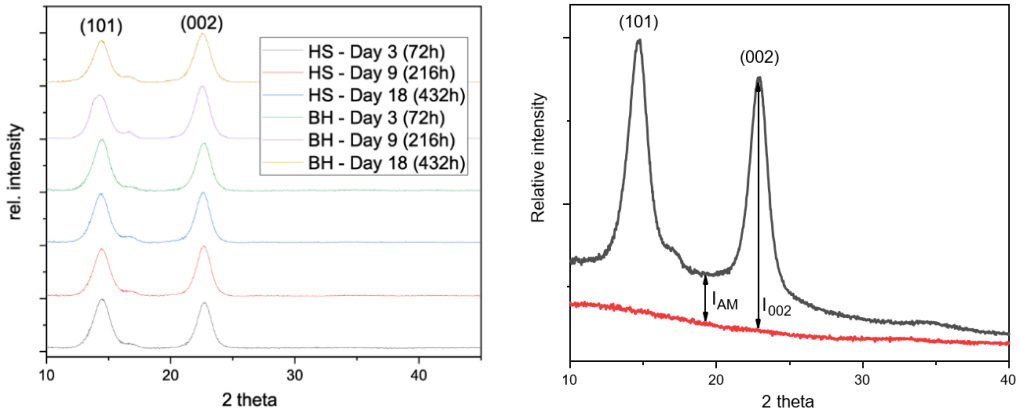
Medium	Time	A_{1427}	A_{898}	LOI	TCI	HBI
HS	Day 3 (72h)	0.03	0.05	0.72	1.87	1.10
	Day 9 (216h)	0.05	0.07	0.70	1.77	1.24
	Day 18 (432h)	0.05	0.08	0.64	1.66	1.18
BH	Day 3 (72h)	0.04	0.06	0.75	1.75	1.00
	Day 9 (216h)	0.04	0.07	0.65	1.73	1.07
	Day 18 (432h)	0.06	0.07	0.81	1.88	1.11

XRD

XRD patterns of all obtained BNC samples revealed two distinct main diffraction peaks at 2θ angles of 14.5° and 22.8°, corresponding to the (101) and (002) crystallographic planes of cellulose Iα and Iβ (Fig. 5a). This showed that BNC synthesized in BH maintained a high degree of crystallinity (CI = 86%) during the active biosynthesis period (72–216 h), comparable to that of the control sample grown in HS. The CS from the peak at 22.8° ranged from 5.8–6.7 nm. However, while CS in the HS sample remained stable (6.7 nm at 72 h and 6.6 nm at 432 h), BNC formed in BH exhibited a gradual decrease in transverse CS: from 6.5 nm (72 h) to 6.1 nm (216 h) and further to 5.8 nm (432 h) (Tab. 4).

This progressive reduction in CS directly confirms the trend identified by FTIR analysis, which showed a 12.8% decrease in LOI during the same active–growth period. This may indicate an accelerated rate of extrusion of individual glucan chains from the terminal complexes of *K. xylinus* DSM 46591, potentially driven by the presence of lignocellulosic products. This process, combined with competing steric interactions at the faces of the growing crystallite, limits the lateral aggregation of elementary microfibrils, resulting in the formation of thinner crystalline domains (5.8–6.1 nm). Upon prolonged incubation (432 h), the 7% lower CI observed in BH samples (CI = 74%) compared to HS samples (CI = 81%) is attributed to the smaller CS (BH 432 h = 5.8 nm). During culture autolysis, the more rigid and robust framework of HS maintains CI, whereas BH undergoes more pronounced local structural rearrangement of the BNC network, leading to a subsequent decrease in CI.

Fig. 5: a) XRD patterns of BNC samples; b) XRD pattern of BH – Day 3 (72 h) illustrating the peak height method for CI calculation; the red line is the background signal measured without cellulose.



Tab. 4: XRD of major parameters of BNC synthesized in HS and BH on days 3, 9, and 18 (72, 216, 432 h).

Medium	Time	Peak position 2θ (°)	Crystallinity index, CI (%)	Crystallite size, CS (nm)
HS	Day 3 (72h)	22.8	86	6.7
	Day 9 (216h)	22.8	79	6.7
	Day 18 (432h)	22.8	81	6.6
BH	Day 3 (72h)	22.8	86	6.5
	Day 9 (216h)	22.8	86	6.1
	Day 18 (432h)	22.8	74	5.8

CONCLUSIONS

This research provides a comprehensive multiscale understanding of the relationship between carbon substrate utilization, crystallographic organization, molecular order, and three–dimensional morphology of the resulting BNC. The developed methodology was demonstrated to stabilize the cultivation conditions of *K. xylinus* DSM 46591 in BH, yielding BNC with physicochemical and structural–morphological characteristics that were better under these particular conditions than those of the material synthesized in HS across the 72–432 h incubation period. Furthermore, it is hypothesized that crude lignocellulosic substrates can serve as effective *in situ* regulators of the supramolecular architectonics of BNC. A scheme of the key metabolic stages governing the distribution of carbon and acetic acid fluxes during BNC biosynthesis by *K. xylinus* DSM 46591 in BH was also proposed, accompanied by a description of the main biochemical steps.

The HPLC analysis confirmed the efficient performance of the BH preparation protocol, verifying stable fermentation kinetics during and after EH and successful target sugar recovery. The FTIR method showed that the optimized BH cultivation microenvironment induces favourable molecular rearrangements: an increase in HBI (0.997→1.111) alongside a controlled 12.8% reduction in LOI. The XRD technique confirmed the preservation of high phase purity for native cellulose Iα and Iβ without cellulose II impurities, showing solid retention of bulk CI compared to HS (CI = 86%) during the active biosynthesis phase (72–216 h). Concurrently, lignocellulosic components in BH are suggested to exert directed *in situ* steric hindrance along the growing (002) crystallographic facets, leading to the formation of finer crystallites (6.1–6.5 nm in BH vs. 6.7 nm in HS). The SEM approach proved that the BNC matrix synthesized in BH formed an open–mesh, highly porous 3D network with preserved capillary porosity. At the extended incubation stage (432 h), substrate depletion and culture autolysis triggered localized erosion of the refined crystalline domains, resulting in a drop in bulk CI to 74%. Overall, the developed protocol for preparing BH is a validated, efficient technological platform that not only stabilizes the bioprocess but also enables higher BNC yields with an enhanced active surface area, higher hydrogen–bonding density, and an optimized porous architecture.

ACKNOWLEDGMENTS

This work was supported by the European Commission within the project LignoSilva [Grant Agreement #101059552] within Horizon Europe Teaming for Excellence.

REFERENCES

1. Akintunde, M.O., Adebayo–Tayo, B.C., Ishola, M.M., Zamani, A., & Horváth, I.S. (2022). Bacterial cellulose production from agricultural residues by two *Komagataeibacter sp.* strains. *Bioengineered*, 13(4): 10010–10025.
2. Amru, A., Luthfi, I., Jahim, J.M., Harun, S., Tan, J.P., Fairuz, S., Manaf, A., Syazwani, S., & Shah, M. (2018). Succinic acid production kinetics. *BioResources* 13(4): 7183–7187.
3. Atalla, R.H., & Vanderhart, D.L. (1984). Native cellulose: a composite of two distinct

crystalline forms. *Science*, 223(4633): 283–285.
4. Chandrasekaran, P.T., Bari, N.K., & Sinha, S. (2017). Enhanced bacterial cellulose production from *Gluconobacter xylinus* using super optimal broth. *Cellulose*, 24(10): 4367–4381.
5. Chorozian, K., Stefanidis, S.D., Kalogiannis, K.G., Lappas, A.A., Topakas, E., & Karnaouri, A. (2026). Production of bacterial nanocellulose from lignocellulosic hydrolysates and its oxidative modification by an AA9 lytic polysaccharide monooxygenase. *Industrial Crops and Products*, 249: 119380.
6. de Amorim, J.D.P., de Souza, K.C., Duarte, C.R., da Silva Duarte, I., de Assis Sales Ribeiro, F., Silva, G.S., de Farias, P.M.A., Stingl, A., Costa, A.F.S., Vinhas, G.M., & Sarubbo, L.A. (2020). Plant and bacterial nanocellulose: production, properties and applications in medicine, food, cosmetics, electronics and engineering. A review. *Environmental Chemistry Letters*, 18(3): 851–869.
7. Domingues, R., Bondar, M., Palolo, I., Queirós, O., Dias de Almeida, C., & Cesário, M.T. (2021). Xylose metabolism in bacteria – opportunities and challenges towards efficient lignocellulosic biomass-based biorefineries. *Applied Sciences,* 11(17): 7800.
8. DSMZ GmbH. (2007). *Gluconobacter oxydans* medium 105. DSMZ, Braunschweig, Germany.
9. Fei, S., Yang, X., Xu, W., Zhang, J., Li, J., Chen, H., Lin, X., Liu, S., & Li, C. (2023). Insights into proteomics reveal mechanisms of ethanol–enhanced bacterial cellulose biosynthesis by *Komagataeibacter nataicola*. *Fermentation*, 9(6): 512.
10. Feng, X., Ullah, N., Wang, X., Sun, X., Li, C., Bai, Y., Chen, L., & Li, Z. (2015). Characterization of bacterial cellulose by *Gluconacetobacter hansenii* CGMCC 3917. *Journal of Food Science*, 80(10): E2217–E2227.
11. French, A.D. (2014). Idealized powder diffraction patterns for cellulose polymorphs. *Cellulose*, 21(2): 885–896.
12. Gorgieva, S., & Trček, J. (2019). Bacterial cellulose: Production, modification and perspectives in biomedical applications. *Nanomaterials,* 9(10): 1352.
13. Kuo, C.H., Chen, J.H., Liou, B.K., & Lee, C.K. (2016). Utilization of acetate buffer to improve bacterial cellulose production by *Gluconacetobacter xylinus*. *Food Hydrocolloids*, 53: 98–103.
14. Mohammadkazemi, F., Azin, M., & Ashori, A. (2015). Production of bacterial cellulose using different carbon sources and culture media. *Carbohydrate Polymers*, 117: 518–523.
15. Montenegro–Silva, P., Ellis, T., Dourado, F., Gama, M., & Domingues, L. (2024). Enhanced bacterial cellulose production in *Komagataeibacter sucrofermentans*: impact of different PQQ–dependent dehydrogenase knockouts and ethanol supplementation. *Biotechnology for Biofuels and Bioproducts*, 17(1): 48.
16. Morales, A., Yang, S., & Salas–de la Cruz, D. (2025). Understanding the morphology of cellulose nanocrystal films via evaporation–induced self–assembly. *ACS Omega*, 10(31): 34930–34940.
17. Motulsky, H., & Christopoulos, A. (2004). Fitting models to biological data using linear and nonlinear regression: a practical guide to curve fitting contents at a glance. GraphPad Software Inc., San Diego, CA, USA.
18. Motulsky, H.J., & Ransnas, L.A. (1987). Fitting curves to data using nonlinear regression:

a practical and nonmathematical review. *FASEB Journal*, 1(5): 365–374.
19. Nelson, M.L. (1964). Relation of certain infrared bands to cellulose crystallinity and crystal lattice type. Part 11. A New infrared ratio for estimation of crystallinity in celluloses I and II. *Journal of Applied Polymer Science,* 8(3): 1325–1341.
20. Nitzsche, R., Grongroft, A., Goj, I., & Kraume, M. (2020). Ultrafiltration of beechwood hydrolysate for concentrating hemicellulose sugars and removal of lignin – Parameter estimation using statistical methods and multiobjective optimization. *Industrial and Engineering Chemistry Research*, 59(16): 7875–7887.
21. Nugroho, D.A., Sutiarso, L., Rahayu, E.S., & Masithoh, R.E. (2022). Kinetics observations of bacterial cellulose thickness formation using an image processing approach during the fermentation process. *Food Research*, 6(1): 210–214.
22. Park, S., Baker, J.O., Himmel, M.E., Parilla, P.A., & Johnson, D.K. (2010). Cellulose crystallinity index: measurement techniques and their impact on interpreting cellulase performance. *Biotechnology for Biofuels,* 3(1): 10.
23. Popescu, C.M., Popescu, M.C., Singurel, G., Vasile, C., Argyropoulos, D.S., & Willfor, S. (2007). Spectral Characterization of Eucalyptus Wood. *Applied Spectroscopy*, 61(11): 1168–1177.
24. Ross, P., Mayer, R., & Benziman, M. (1991). Cellulose biosynthesis and function in bacteria. *Microbiological Reviews,* 55(1): 145–158.
25. ICDD (2022). PDF–2 Database (Release 2022). International Centre for Diffraction Data, Newtown Square, PA, USA.
26. Schramm, M., & Hestrin, S. (1954). Synthesis of cellulose by *Acetobacter xylinum.* Micromethod for the determination of celluloses. *Biochemical Journal*, 56(1): 163–166.
27. Scherrer, P. (1918). Bestimmung der Größe und der inneren Struktur von Kolloidteilchen mittels Röntgenstrahlen. *Nachrichten von der Gesellschaft der Wissenschaften zu Göttingen, Mathematisch–Physikalische Klasse*, 1918: 98–100.
28. Segal, L., Creely, J.J., Martin, A.E., & Conrad, C.M. (1952). Opportunity for new developments in all phases of textile manufacturing. The literature cited an empirical method for estimating the degree of crystallinity of native cellulose using the X–ray diffractometer. *Apparel Manufacturing,* 29(10): 786–794.
29. Shapiro, S.S., & Wilk, M.B. (1965). An analysis of variance test for normality (Complete samples). *Biometrika,* 52(3/4): 591–611.
30. Sugiyama, J., Vuong, R., & Chanzy, H. (1991). Electron diffraction study on the two crystalline phases occurring in native cellulose from an algal cell wall. *Macromolecules*, 24(8): 2116–2122.
31. Tsouko, E., Kourmentza, C., Ladakis, D., Kopsahelis, N., Mandala, I., Papanikolaou, S., Paloukis, F., Alves, V., & Koutinas, A. (2015). Bacterial cellulose production from industrial waste and by–product streams. *International Journal of Molecular Sciences*, 16(7): 14832–14849.
32. Daniel, W.W., & Cross, C.L. (2013). Biostatistics: A Foundation for Analysis in the Health Sciences. 10th ed., John Wiley & Sons, Hoboken, NJ, USA.
33. Meeker, W. Q., & Escobar, L. A. (1998). Statistical methods for reliability data. John Wiley & Sons.
34. Xu, Y., Chi, P., Bilal, M., & Cheng, H. (2019). Biosynthetic strategies to produce xylitol:

an economical venture. *Applied Microbiology and Biotechnology*, 103(13): 5143–5160.
35. Zwietering, M.H., Jongenburger, I., Rombouts, F.M., van 't Riet, K. (1990). Modelling of the bacterial growth curve. *Applied and Environmental Microbiology*, 56(6): 1875–1881.

EDUARD HORBAN*, ALBERT RUSS, ŠTEFAN BOHÁČEK, VLADIMÍR IHNÁT,
ANDREJ PAŽITNÝ, MONIKA STANKOVSKÁ, JÁN TALÁBA
PULP AND PAPER RESEARCH INSTITUTE
DÚBRAVSKÁ CESTA 14, 841 04 BRATISLAVA
SLOVAKIA
*Corresponding author: horban@vupc.sk

PETRA OLEJNÍKOVÁ
SLOVAK UNIVERSITY OF TECHNOLOGY IN BRATISLAVA
FACULTY OF CHEMICAL AND FOOD TECHNOLOGY
INSTITUTE OF BIOCHEMISTRY AND MICROBIOLOGY
812 37 BRATISLAVA
SLOVAKIA

MICHAL ŽITŇAN
ALEXANDER DUBČEK UNIVERSITY OF TRENČÍN
CENTRE FOR FUNCTIONAL AND SURFACE FUNCTIONALIZED GLASS
ŠTUDENTSKÁ 2, 911 50 TRENČÍN
SLOVAKIA